A COLLAPSIBLE IMPULSE RADIATING ANTENNA

Leland H. Bowen[1], Everett G. Farr[1], and William D. Prather[2]

[1]Farr Research, Inc.
 614 Paseo Del Mar, NE
 Albuquerque, NM, USA 87123
[2]Air Force Research Laboratory, Directed Energy Directorate
 3550 Aberdeen Ave. SE
 Kirtland AFB, NM 87117-5776

INTRODUCTION

A reflector Impulse Radiating Antenna (IRA) consists of a parabolic reflector with a TEM feed. The IRA provides broadband coverage with a narrow beamwidth. This class of antenna has a considerable body of literature associated with both its analysis and measurements[1,2,3]. Farr Research, Inc. has developed a Collapsible Impulse Radiating Antenna (CIRA) with outstanding RF characteristics. The approach selected by Farr Research for the FRI-CIRA-1 utilizes an umbrella-like design, with a reflector sewn from a very tough, electrically conductive mesh fabric. The CIRA is lightweight, compact, and easily portable with low wind loading and high mechanical ruggedness.

The reflector for the FRI-CIRA-1 is 1.22 m (4 feet) in diameter with a focal length of 0.488 m (F/D = 0.4). The antenna, when collapsed, measures 102 mm (4 in) in diameter by 810 mm (32 in) long. The antenna weighs 2 kg (4.5 lb.).

We measured the characteristics of the antenna using the time domain outdoor antenna range of Farr Research. The time domain data were processed to obtain the normalized time domain impulse response (TDIR) as described by Farr and Baum[4] and summarized in the next section of this paper. We made pattern measurements at 2.5° intervals in both the H and E planes and converted them to effective gain. The conversion from impulse response to effective gain is based on the derivation given by Bowen *et al*,[5] and summarized later in this paper. We present the impulse response characteristics in both the time and frequency domains. We also present the effective gain on boresight as a function of frequency. Finally, we present the effective gain as a function of angle in the principal planes, at multiple constant frequencies.

Normalized Impulse Response

Before we get into the details of the antennas, we first review the parameters used to describe them. We can describe antennas in the time domain with an impulse response, of the form $h_N(t)$. Here we provide a quick review of the derivation by Farr and Baum.[4] We use somewhat simplified antenna equations that show only the response to dominant polarization on boresight without the propagation terms. It is straightforward to add these other effects later.

In transmission mode, the antenna radiates a field on boresight, $E_{rad}(t)$, which is described by

$$\frac{E_{rad}(t)}{\sqrt{Z_o}} = \frac{1}{2\pi r c} h_N(t) \circ \frac{1}{\sqrt{Z_c}} \frac{dV_{src}(t)}{dt} \tag{1}$$

where Z_o = 376.7 Ω is the impedance of free space, Z_c is the impedance of the 50 Ω feed cable, r is the distance to the observation point on boresight, $V_{src}(t)$ is the source voltage measured into a 50 Ω load, c is the speed of light in free space, and the " $\circ$ " symbol indicates convolution. In reception mode, the antenna is described by

$$\frac{V_{rec}(t)}{\sqrt{Z_c}} = h_N(t) \circ \frac{E_{inc}(t)}{\sqrt{Z_o}} \tag{2}$$

where $E_{inc}(t)$ is the incident electric field on boresight. Note that the normalized impulse response, $h_N(t)$, completely describes the behavior of any antenna in both transmission and reception. If we have both a transmitting and receiving antenna, we can relate the received voltage to the source voltage by combining the above two equations as

$$V_{rec}(t) = \frac{1}{2\pi r c} h_{N,RX}(t) \circ h_{N,TX}(t) \circ \frac{dV_{src}(t)}{dt} \tag{3}$$

where $h_{N,RX}(t)$ is the normalized impulse response of the receive antenna and $h_{N,TX}(t)$ is the corresponding response of the transmit antenna.

To calibrate our measurement system, we use two identical TEM sensors. In this case, the combined antenna equation becomes

$$V_{rec}(t) = \frac{1}{2\pi r c} h_{N,tem}(t) \circ h_{N,tem}(t) \circ \frac{dV_{src}(t)}{dt} \tag{4}$$

The normalized frequency domain impulse response of the sensors can be extracted from (4) as

$$\widetilde{h}_{N,tem}(\omega) = \sqrt{\frac{2\pi r c \widetilde{V}_{rec}(\omega)}{j\omega \widetilde{V}_{src}(\omega)}} \tag{5}$$

Once a calibration has been performed with two identical antennas, then we can measure the response of an antenna under test (AUT) by replacing one of the sensors with the antenna under test. The impulse response of the antenna then becomes

$$\widetilde{h}_{N,AUT}(\omega) = \frac{2\pi r c \widetilde{V}_{rec}(\omega)}{j\omega \widetilde{V}_{src}(\omega) h_{N,tem}(\omega)} \tag{6}$$

and the time domain normalized impulse response is found with an inverse Fourier transform.

When making measurements on a focused aperture antenna, we normally extract an aperture height, h_a, which can be related to the physical parameters of the AUT. However, h_a is difficult to measure directly, without making assumptions about the antenna's feed impedance, so we will first find the effective height, h_{eff}. The effective

height is useful since (at midband) it relates the incident electric field strength (in V/m) to the voltage into a scope ($V_{rec}(t)$, in volts) by a simple proportionality

$$V_{rec}(t) \approx h_{eff} \, E_{inc}(t) \tag{7}$$

This expression is valid only when the full-width half-max (FWHM) of $h_N(t)$ is much less than the measured signal. The midband effective height can be determined from (2) and the integral of the impulsive portion of the normalized impulse response, and it is calculated as

$$h_{eff} = \sqrt{\frac{Z_c}{Z_o}} \int_{Impulse} h_N(t) \, dt \tag{8}$$

where the integral is over the impulsive part of $h_N(t)$. Once we have h_{eff}, we can convert it to h_a using

$$h_a = h_{eff} \, / \, \tau_{RX} \tag{9}$$

where

$$\tau_{RX} = \frac{2 \, Z_c}{Z_c + Z_a} \tag{10}$$

In these equations, Z_a is the antenna feed impedance on the TEM portion of the feed arms, and τ_{RX} is the transmission coefficient between the TEM feed arms and the feed cable. Note that the quantity h_a is meaningful only in the context of a wideband antenna with a TEM feed. Note also that the quantity h_a is impossible to measure directly – one can only approximate it after assuming that the feed impedance is a constant across the relevant bandwidth, and is purely resistive. On the other hand, we can measure h_{eff} without making approximations, as long as the time domain impulse response has an impulse-like wave shape. For this reason, h_{eff} provides a more useful description of antenna performance than h_a.

Note also that when there is a balun in the circuit, a different form of the transmission coefficient must be used. For example, in the case of the IRA, there is a balun that matches the 200 Ω impedance of the antenna to a 50 Ω cable, using two sections of 100 Ω transmission line connected in parallel at one end and in series at the other end. In this case, the voltage is halved, so the transmission coefficient, τ_{RX}, is 0.50. The use of h_{eff} avoids this difficulty, by avoiding the need to define the transmission coefficient.

EFFECTIVE GAIN

It is frequently desirable to convert the impulse response developed in the previous section to frequency domain gain as defined by in IEEE Std 145.[7] As we will see, for wideband applications the effective gain is a more useful quantity, because it accounts for impedance mismatch between the antenna port and feed cable. We provide here the derivation of effective gain from the normalized impulse response, $h_N(t)$.[5]

We begin with the standard expressions in the frequency domain. Thus, the power received into a 50-ohm feed cable is

$$P_{rec} = \varepsilon \, A_{eff} \, S_{inc} \tag{11}$$

where S_{inc} is the incident power density in W/m^2, A_{eff} is the effective area, and ε is a power transmission coefficient that accounts for the impedance mismatch between the antenna port and 50-ohm feed cable. Absolute gain is related to effective aperture by

$$A_{eff} = \frac{\lambda^2}{4\pi} G = \frac{\lambda^2}{4\pi} \frac{G_{eff}}{\varepsilon} \tag{12}$$

where G_{eff} is the effective gain, the gain after accounting for the impedance mismatch between the antenna port and the 50-ohm feed cable. The term "effective gain" has not yet been recognized by the IEEE Std. 145[7], but it is in common use[8]. Combining the above two equations, we have

$$P_{rec} = \frac{\lambda^2 G_{eff}}{4\pi} S_{inc} \tag{13}$$

By taking the square root, and recasting into voltages, we find

$$\frac{V_{rec}(\omega)}{\sqrt{Z_c}} = \frac{\lambda \sqrt{G_{eff}(\omega)}}{2\sqrt{\pi}} \frac{E_{inc}(\omega)}{\sqrt{Z_o}} \tag{14}$$

where Z_c is the cable impedance (generally 50 Ω) and Z_O is the impedance of free space, 376.727 Ω.

Let us now compare the above equation to the standard equation for reception. Thus, we convert (2) of this paper into the frequency domain, obtaining

$$\frac{V_{rec}(\omega)}{\sqrt{Z_c}} = h_N(\omega) \frac{E_{inc}(\omega)}{\sqrt{Z_o}} \tag{15}$$

where $h_N(\omega)$ is the normalized antenna impulse response expressed in the frequency domain. The normalized impulse response, $h_N(t)$, is already known. To convert it to effective gain, we combine equations (14) and (15),

$$\boxed{G_{eff}(\omega) = \frac{4\pi}{\lambda^2} |h_N(\omega)|^2 = \frac{4\pi f^2}{c^2} |h_N(\omega)|^2} \tag{16}$$

This formula allows us to convert our time domain normalized impulse response to effective gain, and this is the formula that is used in the remainder of this paper. Effective gain is simply absolute gain, as defined by IEEE Std. 145, multiplied by a transmission coefficient that accounts for mismatch between the antenna and feed line. For ultra-wideband (UWB) antennas, this is a far more useful version of gain than simple antenna gain (or absolute gain) as defined by IEEE Std. 145. This is due to the fact that impedance mismatch between the antenna and feed line is a large part of the challenge inherent in UWB antenna design.

CIRA DESCRIPTION

Let us now provide details of the design of the CIRA. The cross section of the CIRA is shown in Figure 1, and a photograph of the open CIRA is shown in Figure 2. The reflector for the FRI-CIRA-1 is 1.22 m (48 in) in diameter with a focal length of 0.488 m (F/D = 0.4) The parabolic reflector is constructed of a very tough electrically conductive mesh fabric. This fabric is silver and nickel plated and has a resistivity of less than 0.2 Ω/square. The wind loading on the antenna is low due to the high air permeability of the fabric. The reflector has 12 sections or panels that are supported on an umbrella-like frame with fiberglass stays. The stays are connected to the support at the rear of the antenna by aluminum pivots. The antenna is opened by sliding the yoke on the center rod toward the rear of the antenna. Turning the knob on the yoke locks the antenna open.
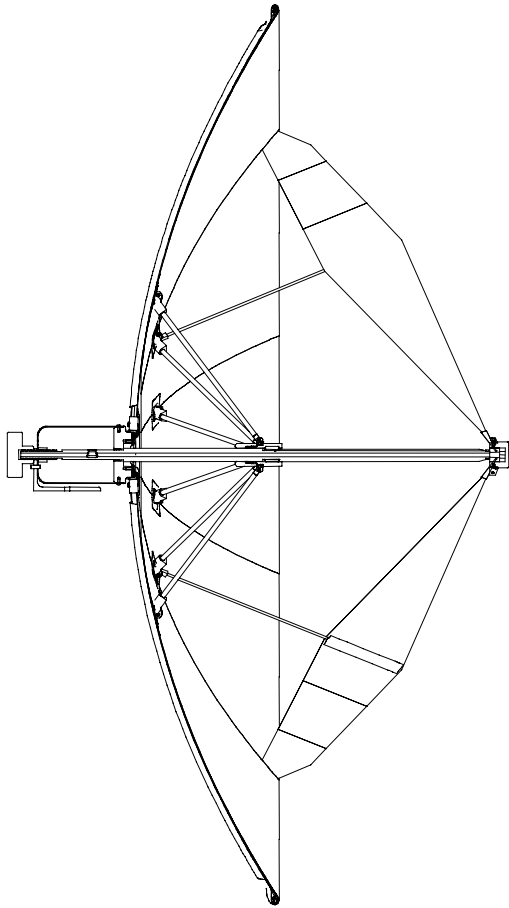
Figure 1. CIRA cross section.

Figure 2. FRI-CIRA-1.

An aluminum enclosure located at the rear center of the antenna houses the RF splitter and acts as the support for the antenna. The splitter was provided by Prodyn Technologies. It consists of a 50 Ω input impedance connector, which then splits into two 95 Ω cables. The cables attach to the feed arms at the feed point in a series/parallel configuration as is standard for IRAs with 4 feed arms. The feed arms are made from a combination of conductive rip-stop nylon and resistive (~200 Ω/square) polyester fabric. The feed arms are attached to copper tips that facilitate the necessary solder connections at the feed point. The copper tips are attached to a Teflon support on the end of the center rod. A cover made from ultra-high molecular weight polyethylene (UHMW) protects the electrical connections at the feed point. An SMA connector on the side of the splitter enclosure provides a 50 Ω connection to the antenna. A bracket attached to the splitter enclosure provides a standard 3/8″-16 thread tripod connection. The antenna can be rotated easily to either horizontal or vertical polarization by repositioning the tripod support bracket. The backside of the antenna with the splitter enclosure and tripod mount is shown in Figure 3. The large black knob shown to the right of the picture can be loosened to reposition the tripod bracket. Also shown in this figure is one of the coaxial cables between the splitter and the feed point.

The collapsed antenna is shown in Figure 4. When collapsed, the antenna measures 102 mm (4 in.) diameter by 810 mm (32 in.) long. The antenna weighs 2 kg (4.5 lb.) and can be easily transported and set up by one person.

Figure 3. Splitter enclosure.   Figure 4. Collapsed CIRA-1

CIRA DATA

We measured the characteristics of the CIRA-1 using the time domain outdoor antenna range of Farr Research. The FRI-TEM-2-100 horn sensor used for these measurements is a standard sensor manufactured by Farr Research. These sensors are ultra-wideband electric field sensors designed for low dispersion and high sensitivity. They are calibrated using two identical sensors and the normalized impulse response procedure described earlier. The impulse response of this 100 Ω sensor has a FWHM of 47 ps. The clear time is 4 ns. The midband effective height of the sensor is 42 mm. These sensors overcome the problem of making fast impulse field measurements with derivative sensors, which have very low sensitivity and small effective areas at high frequencies. The TEM sensors are a half TEM horn mounted on a truncated ground plane. Four versions of TEM horn sensors are available from Farr Research[9].

We used a Picosecond Pulse Labs 4015C step generator to drive the TEM horn antenna. This step generator has a 4 V output with a 25 ps risetime. The response of the CIRA-1 was recorded using a Tektronix 11801B Digital Oscilloscope with a SD-24 TDR/Sampling Head. The distance between the antennas was 20 m and the height was 3 m. We measured the antenna pattern in the H and E planes at 2.5° increments from 0° to 45° off boresight. Also, the effective gain is computed and plotted on boresight as a function of frequency and at various frequencies as a function of angle in the principal planes.

The test data for the CIRA-1 are as follows. The TDR of the CIRA is shown in Figure 5. The TDR at the feed point and along the feed arms is the best (flattest) we have achieved on this type antenna. In Figures 6–10 we show the on-boresight characteristics of the CIRA-1. The data were clipped just before the arrival of the ground bounce signal and then zero-padded out to 20 ns to provide frequency domain information down to 50 MHz. The FWHM of the normalized impulse response (Figure 7) is 70 ns. The CIRA proved to be usable from below 50 MHz to above 8 GHz, as shown in Figures 8 and 9.

When deciding the distance at which to place the sensor, one has to realize that the far-field begins at a distance that is dependent upon the smallest FWHM one expects to measure. We expected a FWHM of around 100 ps, so we expected that a distance of 20 meters would be adequate. However, we were pleasantly surprised by the 70ns FWHM measurements of the improved CIRA. This narrower impulse width extends the far field to around 25 m, using the formula $r > (3/2) a^2 /(c\, t_{FWHM})$, where a is the antenna radius, c is the speed of light in free space, and t_{FWHM} is the FWHM of the

radiated impulse response. While there was no opportunity to make new measurements at a greater distance, we believe the measurement error due to antenna spacing is small.

Next, we provide the effective gain vs. frequency in Figure 10. These data show that at lower frequencies the response of this antenna is quite flat and that the high-frequency response is approximately smooth to 8 GHz. The peak effective gain of the CIRA is 23 dB at 4 GHz. The midband effective height of the antenna is found from the integral of the normalized impulse response shown in Figure 9 to be approximately 0.28 m ($h_{eff} = 0.38\sqrt{50/377}, h_a = h_{eff}/0.5$). This is 71 % of the theoretical value of 0.396 m.
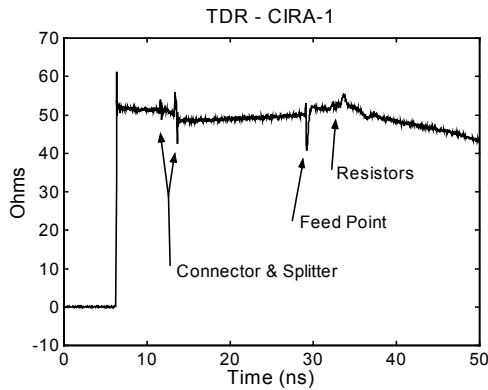
Figure 5. TDR of CIRA-1.
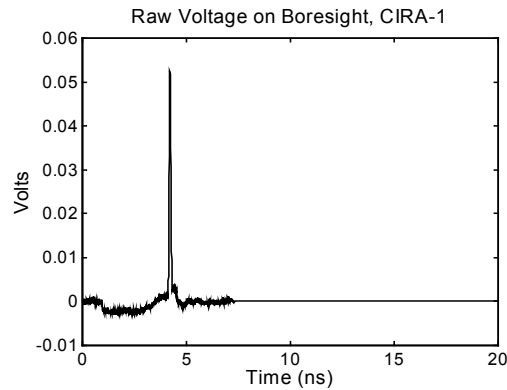
Figure 6. Zero padded response.
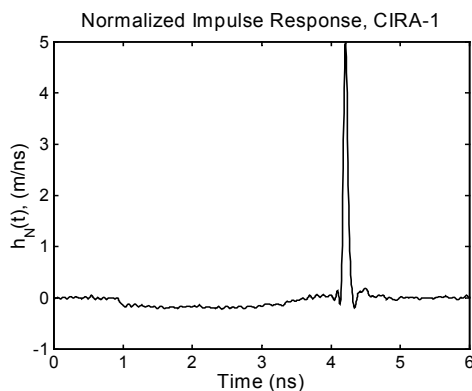
Figure 7. Expanded Impulse Response.
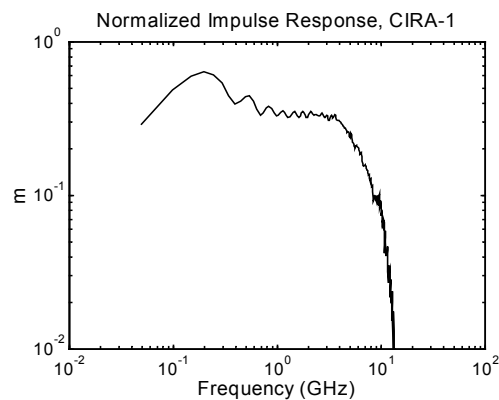
Figure 8. Frequency domain response.
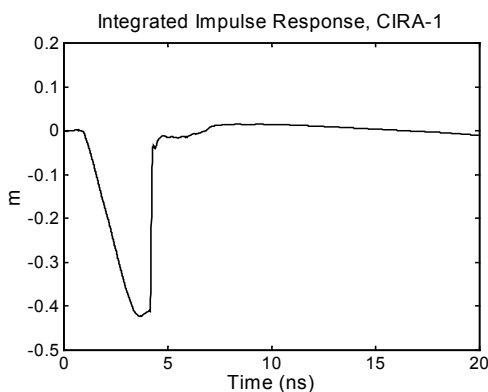
Figure 9. Integral of impulse response.
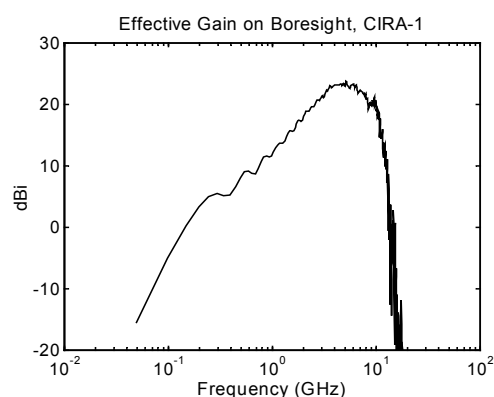
Figure 10. Standard gain on boresight.

In Figure 11 we show the cross-polarization (crosspol) response of the CIRA. The effective gain on boresight for the crosspol case is shown in Figure 12. The crosspol response is 10–20 dB below the copol response from Figure 10. This data may be of interest due to recent work suggesting improvements in the IRA that would result in improved gain and reduced crosspol.[6] This is accomplished by placing the feed arms

at ±30° from vertical, instead of ±45°, which we currently have in the CIRA. We have recently demonstrated this principle on an 18-inch diameter IRA with an aluminum dish with great success. Since each panel of the CIRA is 30° wide, it will be straightforward to incorporate the new feed arm positions into future versions of the CIRA.
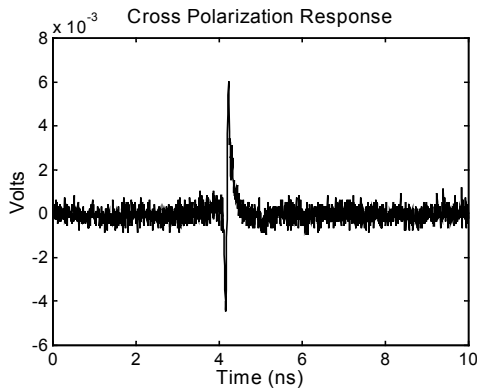

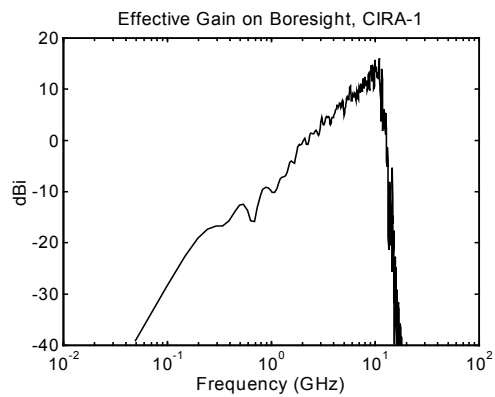Figure 11. Raw cross polarization response.

Figure 12. Cross polarization gain.

Next, in Figures 13–14 we show the antenna pattern in the H and E planes, based on the peaks of the raw voltage measurements. The half-voltage beamwidth is 5.1° in the H plane and 6° in the E plane. If we choose to use the half-power beamwidth, we have ~3° in both the H and E planes. Samples of the raw data from the H and E plane scans are shown in Figures 15–16.
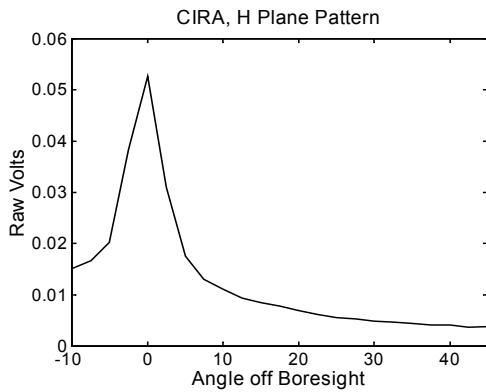
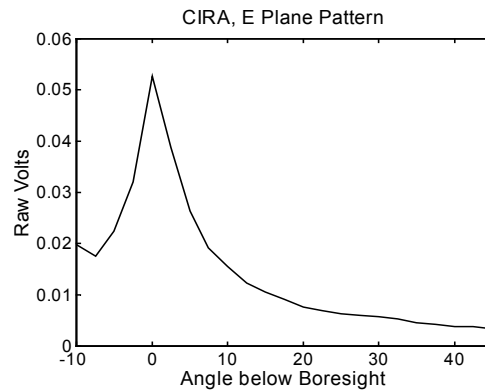Figure 13. Antenna pattern in H plane.
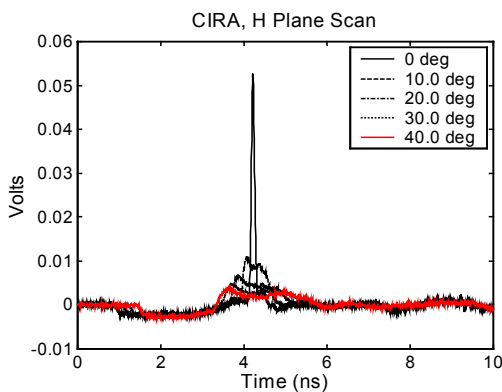

Figure 14. Antenna pattern in E plane.

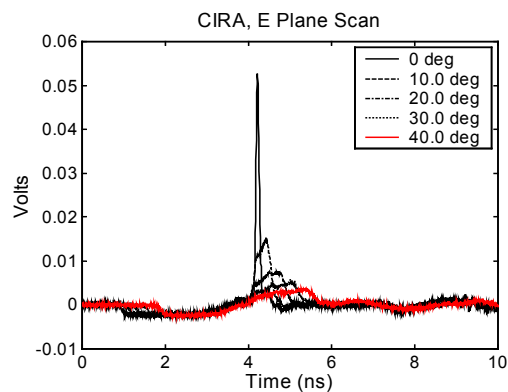Figure 15. Samples from H plane scan.

Figure 16. Samples from E plane scan.

In Figures 17–18 we show the principal plane pattern cuts of the antenna at various frequencies. At low frequencies, the pattern is quite smooth and flat as expected. At high frequencies the high gain and narrow beam width become evident.
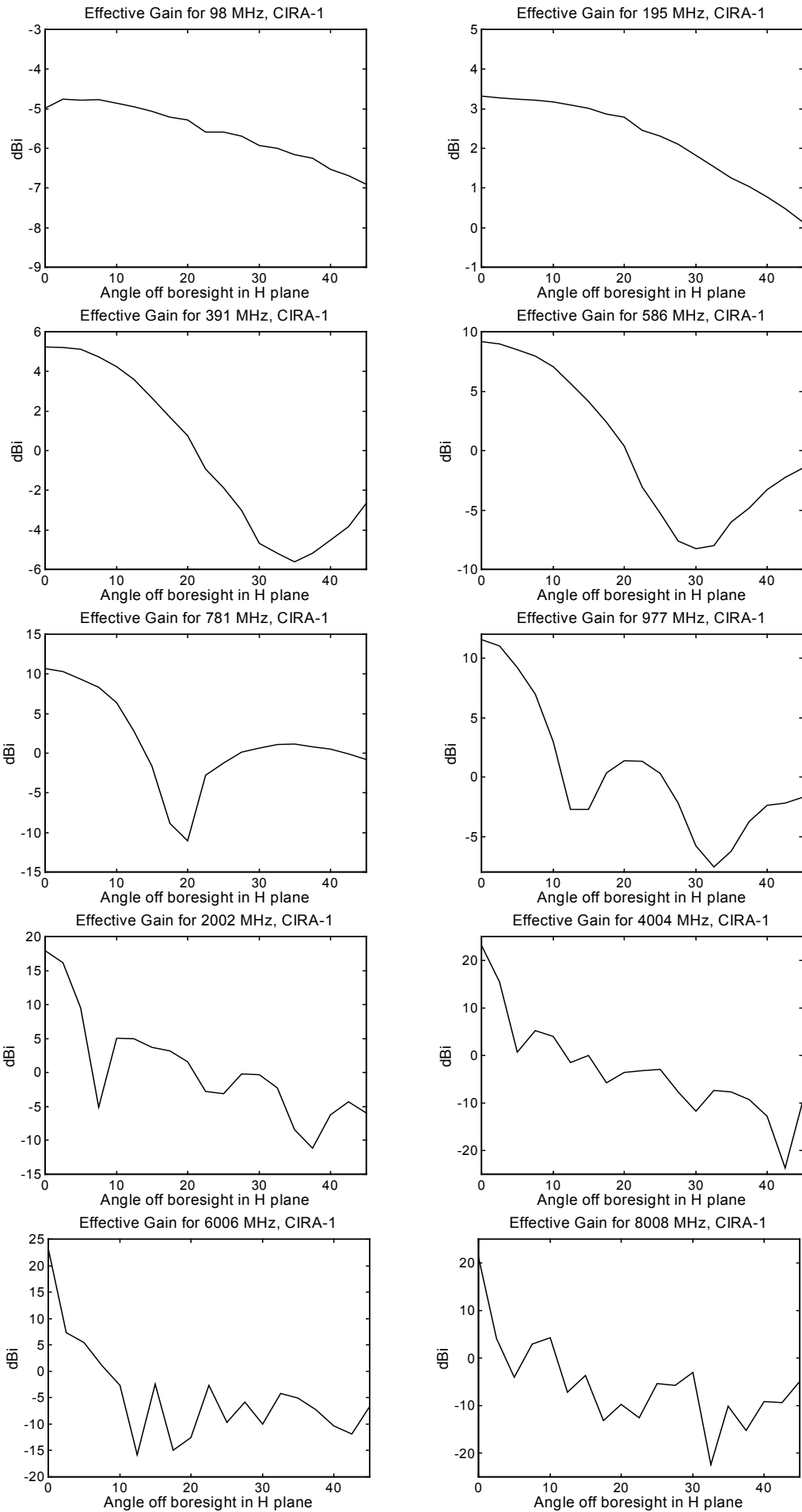
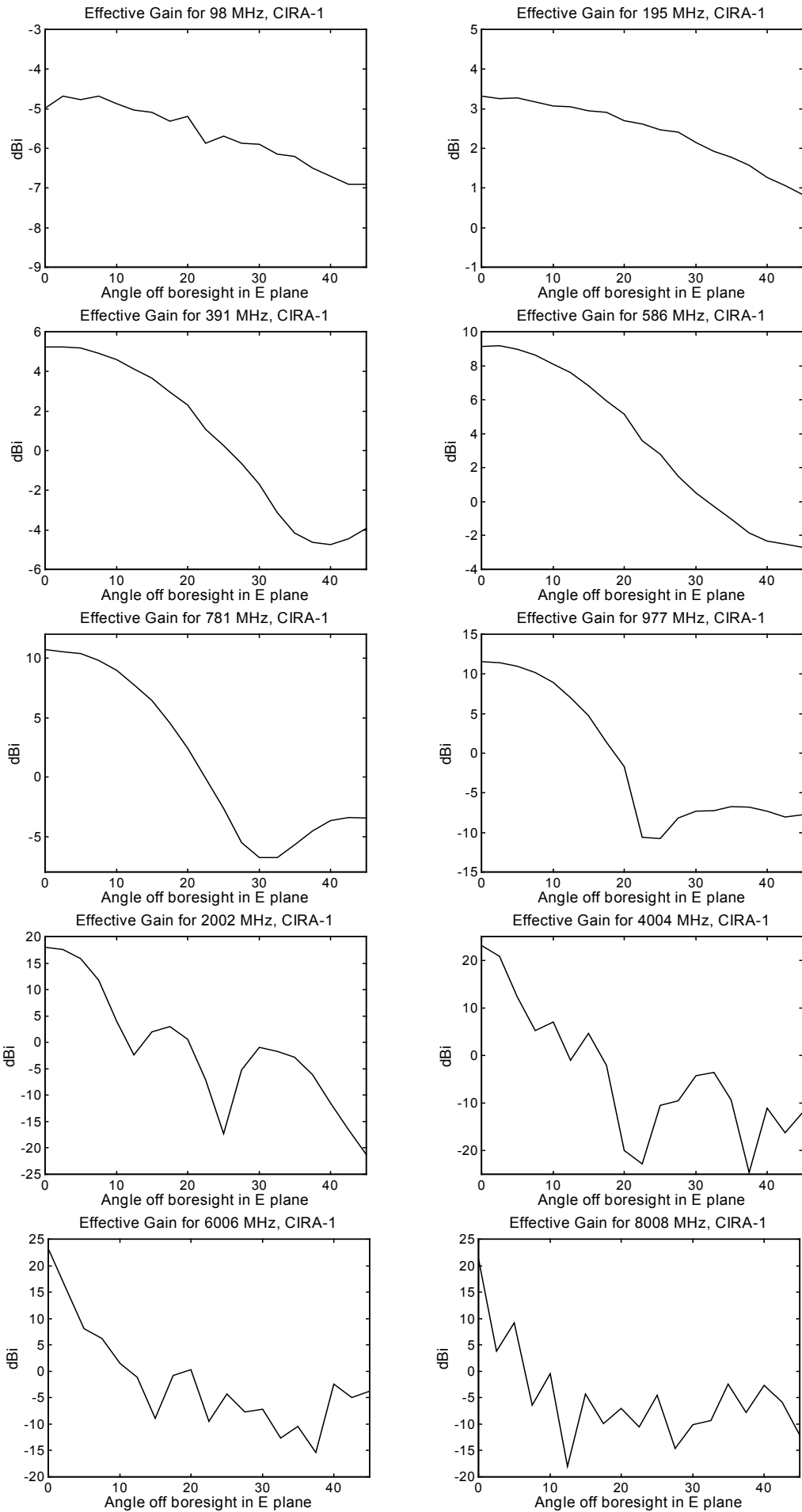Figure 17. Effective gain vs. angle off boresight in H plane.

Figure 18. Effective gain vs. angle off boresight in E plane.

CONCLUSION

The FRI-CIRA-1 provides broadband antenna coverage in a single compact package that is easily portable.

The antenna has outstanding RF characteristics in both the frequency and time domains. In the time domain, it has an impulse response with FWHM of 70 ps and mid-band effective height h_{eff} = 30 cm. In the frequency domain, the peak effective gain at 4 GHz is 23 dBi, and the antenna is usable from 50 MHz to 8 GHz.

The reflector for the FRI-CIRA-1 is 1.22 m (4 feet) in diameter with a focal length of 0.488 m (F/D = 0.4). The umbrella-like frame covered with conductive mesh fabric provides a very practical, lightweight, and easy-to-use antenna. The collapsed antenna measures 102 mm (4 in) diameter x 810 mm (32 in) long. The antenna weighs 2 kg (4.5 lb.). The antenna can be easily transported and set up by one person and can be attached to a variety of military and commercial off-the-shelf transmitters and receivers. The FRI-CIRA-1 is now commercially available from Farr Research, Inc.

Patent Notice

A patent is pending on the antenna described in this paper.

REFERENCES

1. C. E. Baum and E. G. Farr, Impulse Radiating Antennas, pp. 139-148 in H. L. Bertoni *et al* (eds.), *Ultra-Wideband, Short-Pulse Electromagnetics*, New York, Plenum Press, 1993.
2. E. G. Farr, C. E. Baum, and C. J. Buchenauer, Impulse Radiating Antennas, Part II, pp. 159-170 in L. Carin and L. B. Felsen (eds.), *Ultra-Wideband, Short-Pulse Electromagnetics 2*, New York, Plenum Press, 1995.
3. E. G. Farr, C. E. Baum, and C. J. Buchenauer, Impulse Radiating Antennas, Part III, pp. 43-56 in C. E. Baum *et al* (eds.), *Ultra-Wideband, Short-Pulse Electromagnetics 3*, New York, Plenum Press, 1997.
4. E. G. Farr and C. E. Baum, Time Domain Characterization of Antennas with TEM Feeds, Sensor and Simulation Note 426, October 1998.
5. L. H. Bowen, E. G. Farr, and W. D. Prather, Fabrication and Testing of Two Collapsible Impulse Radiating Antennas, Sensor and Simulation Note 440, November 1999.
6. J. S. Tyo, Optimization of the Feed Impedance for an Arbitrary Crossed-Feed-Arm Impulse Radiating Antenna, Sensor and Simulation Note 438, November 1999.
7. IEEE, *IEEE Standard Definition of Terms for Antennas*, IEEE Std 145-1993, Institute for Electrical and Electronics Engineering, Inc., New York, March 1993.
8. George H. Hagn, Personal communication, January 2000.
9. L. H. Bowen and E. G. Farr, Recent Enhancements to the Multifunction IRA and TEM Sensors, Sensor and Simulation Note 434, February 1999.